

W-PAIR PRODUCTION IN THE PROCESS $e^+e^- \rightarrow \ell\nu q\bar{q}'$ AND MEASUREMENT OF THE $WW\gamma$ and WWZ COUPLINGS

Mikuláš Gintner and Stephen Godfrey*

Ottawa-Carleton Institute for Physics

Department of Physics, Carleton University, Ottawa CANADA, K1S 5B6

Gilles Couture†

Département de Physique, Université du Québec à Montréal

C.P. 8888, Succ. Centre-Ville, Montréal, Québec, Canada, H3C 3P8

We performed a detailed analysis of the process $e^+e^- \rightarrow \ell\nu q\bar{q}'$ where we included all tree level Feynman diagrams that contribute to this final state. We studied the sensitivity of this process to anomalous trilinear gauge boson couplings of the $WW\gamma$ and WWZ vertices using two popular parametrizations. We used a maximum likelihood analysis of a five dimensional differential cross-section based on the W and W decay product angular distributions. We concentrated on LEP-200 energies, taking $\sqrt{s} = 175$ GeV, and energies appropriate to the proposed Next Linear Collider (NLC), a high energy e^+e^- collider with center of mass energies $\sqrt{s} = 500$ and 1 TeV. At 175 GeV, g_1^Z can be measured to about ± 0.2 , κ_Z to ± 0.2 and κ_γ to ± 0.3 , λ_Z to ± 0.2 and λ_γ to ± 0.3 . at 95% C.L. assuming 500 pb⁻¹ integrated luminosity. Although these will be improvements of existing measurements they are not sufficiently precise to test the standard model at the loop level and are unlikely to see deviations from SM expectations. At 500 GeV with 50 fb⁻¹ integrated luminosity, g_1^Z can be measured to about ± 0.01 , κ_Z and κ_γ to ± 0.005 and λ_Z and λ_γ to ± 0.003 at 95%

C.L. while at 1 TeV with 200 fb^{-1} integrated luminosity, κ_V and λ_V can be measured to about ± 0.005 and $\pm 10^{-3}$ respectively. The 500 GeV measurements will be at the level of loop contributions to the couplings and may show hints of new physics while the 1 TeV should be sensitive to new physics at the loop level.

PACS numbers: 13.10.+q, 14.70.-e

I. INTRODUCTION

e^+e^- colliders have made important contributions to our understanding of the electroweak interactions [1] and it is expected that this tradition will continue with the advent of higher luminosity and higher energy machines. In the near future the CERN LEP-200 e^+e^- collider [2–4] will begin operation and beyond that there is a growing effort directed towards the design and construction of future high energy e^+e^- linear colliders with $\sqrt{s} \geq 500$ GeV which we will refer to generically as the Next Linear Collider (NLC) [5–10]. One of the primary physics goals of LEP-200 and an important goal of the NLC is to make precision measurements of W boson properties including M_W , Γ_W , and W -boson interactions with fermions and the photon and Z^0 .

The latter measurements, that of the trilinear gauge boson vertices (TGV's) provides a stringent test of the gauge structure of the standard model [11,12]. The current measurement of these couplings are rather weak. Using a popular parametrization of the CP conserving gauge boson couplings, indirect measurements of TGV's via radiative corrections to precision electroweak measurements [13–15] give the following limits [13]: $\delta g_Z^1 = -0.033 \pm 0.031$, $\delta\kappa_\gamma = 0.056 \pm 0.056$, $\delta\kappa_Z = -0.0019 \pm 0.044$, $\lambda_\gamma = -0.036 \pm 0.034$, and $\lambda_Z = 0.049 \pm 0.045$. However, there are ambiguities in these calculations associated with running the couplings down from the scale of new physics to low energy so that these limits are not particularly rigorous and it is necessary to use direct measurements for more reliable bounds. The CDF and D0 collaborations at the Tevatron $p\bar{p}$ collider at Fermilab, using the processes $p\bar{p} \rightarrow W\gamma$, WW , WZ , have obtained the direct 95% C.L. limits of $-1.6 < \delta\kappa_\gamma < 1.8$, $-0.6 < \lambda_\gamma < 0.6$, $-8.6 < \delta\kappa_Z < 9.0$, and $-1.7 < \lambda_Z < 1.7$ [16]. These measurements are quite weak but it is expected that they will improve as the luminosity of the Tevatron increases. In the longer term measurements at the Large Hadron Collider at CERN will improve these limits considerably [17].

It is expected that measurements at high energy e^+e^- colliders will surpass those at the hadron colliders. As a result, many processes have been studied to determine their

usefulness for measuring the TGV's; $e\gamma \rightarrow \nu W$ [18–21], $e^-e^- \rightarrow e^-W^-\nu_e$ [22], $\gamma\gamma \rightarrow W^+W^-$ [18,23], $e^+e^- \rightarrow Z\nu\bar{\nu}$ [24–26], $e^+e^- \rightarrow \gamma\nu\bar{\nu}$ [6,27,28], $e^+e^- \rightarrow W^+W^-$ [2,11,29–33] and more detailed studies of various four fermion final states in the process $e^+e^- \rightarrow W^+W^- \rightarrow f\bar{f}f'\bar{f}'$ [34,24,35,36].

Probably the most useful of the $e^+e^- \rightarrow W^+W^-$ channels for these studies is $e^+e^- \rightarrow \ell\nu q\bar{q}'$. With only one unobserved neutrino this channel has several advantages: it can be fully reconstructed using the constraint of the initial beam energies, the W^+ and W^- can be discriminated using lepton charge identification, it does not have the QCD backgrounds that plague the fully hadronic decay modes, and it offers much higher statistics than the fully leptonic modes. As a result of the importance of this channel there have been numerous studies of this process. In particular, there is a growing list of analysis of $e^+e^- \rightarrow W^+W^-$, e^+e^- to four fermion final state processes [11,24,35,30,37,38], single W production [26,39], electroweak radiative corrections to these reactions including the important contribution from initial state radiation [40–45], and the sensitivity of these processes to anomalous $WW\gamma$ and WWZ^0 gauge boson couplings (TGV's).

In this paper we examine in detail the four fermion final state $e^+e^- \rightarrow \ell\nu_\ell q\bar{q}'$ where ℓ is either e^\pm or μ^\pm and $q\bar{q}'$ can be either (ud) or (cs) . We study this process for the centre of mass energies $\sqrt{s} = 175$ GeV appropriate to LEP200, and $\sqrt{s} = 500$ and 1000 GeV appropriate to the NLC. To obtain results we included all tree level diagrams to the four fermion final states using helicity amplitude techniques. For the $\mu^\pm\nu_\mu q\bar{q}'$ final state 10 diagrams contribute and for the $e^\pm\nu_e q\bar{q}'$ final state 20 diagrams contribute. Our primary interest is to study the sensitivity of these processes to anomalous gauge boson couplings. To do so we examined numerous distributions. For the purpose of comparing theory to experiment we also examined the question of whether the approximation of only including the resonant diagrams is adequate or whether the full four-fermion final state calculation is needed. Using helicity amplitudes we are able to study the usefulness of initial state polarization in extracting the TGV's. In the $e^\pm\nu q\bar{q}'$ final state single W production can also be studied [39] where the $WW\gamma$ vertex can be isolated from the WWZ vertex by imposing

an appropriate cut on the outgoing electron. In this case, when only hadronic jets are observed and not the outgoing lepton, there are ambiguities in identifying the charge of the W besides problems with hadronic backgrounds which we do not deal with here. A detailed analysis of single W production will be presented elsewhere [46].

In the next section we discuss effective Lagrangians and the various parametrizations used to describe gauge boson self interactions which have appeared in the literature. In section III we describe our calculation. Section IV comprises the bulk of the paper which is used to present and discuss our results. We summarize our conclusions in section V.

II. PARAMETRIZATION OF THE TRIPLE GAUGE BOSON COUPLINGS

The formalism of effective Lagrangians provides a well-defined framework for investigating the physics of anomalous couplings and electroweak symmetry breaking [11,47,48]. In this approach an infinite set of non-renormalizable operators, consistent with the unbroken symmetries and whose coefficients parametrize the low-energy effects of electroweak symmetry breaking or new physics are organized in an energy expansion. At low energy only a finite number of terms contribute to a given process. At higher energies more and more terms become important until the whole process breaks down at the scale of new physics. One focuses on the leading operators in the expansion.

There are three main parametrizations of gauge boson couplings that appear in the literature. The characteristic distinguishing the approaches is the degree to which constraints are imposed in terms of the symmetry and particle content of the low energy theory. We summarize the most commonly used parametrizations below [11,47].

A. General Form Factor Approach

The first approach is to describe the WWV vertices using the most general parametrization possible that respects Lorentz invariance, electromagnetic gauge invariance and CP

invariance [2,49,50]. This approach has become the standard parametrization used in phenomenology making the comparison of the sensitivity of different measurements to the TGV's straightforward. We do not consider CP violating operators in this paper as they are tightly constrained by measurement of the neutron electric dipole moment which constrains the two CP violating parameters to $|\tilde{\kappa}|, |\tilde{\lambda}| < \mathcal{O}(10^{-4})$ [51]. With these constraints the $WW\gamma$ and WWZ vertices have five free independent parameters, g_1^Z , κ_γ , κ_Z , λ_γ and λ_Z and is given by [2,49]:

$$\mathcal{L}_{WWV} = -ig_V \left\{ g_1^V (W_{\mu\nu}^+ W^{-\mu} - W^{+\mu} W_{\mu\nu}^-) V^\nu + \kappa_V W_\mu^+ W_\nu^- V^{\mu\nu} + \frac{\lambda_V}{M_W^2} W_{\lambda\mu}^+ W_\nu^- V^{\nu\lambda} \right\} \quad (1)$$

where the subscript V denotes either a photon or a Z^0 , V^μ and W^μ represents the photon or Z^0 and W^- fields respectively, $W_{\mu\nu} = \partial_\mu W_\nu - \partial_\nu W_\mu$ and $V_{\mu\nu} = \partial_\mu V_\nu - \partial_\nu V_\mu$ and M_W is the W boson mass. (g_1^Z is constrained by electromagnetic gauge invariance to be equal to 1.) The first two terms correspond to dimension 4 operators and the third term corresponds to a dimension 6 operator. The mass in the denominator of the dimension 6 term would correspond to the scale of new physics, typically of order 1 TeV. However, it has become the convention to use M_W so that the W magnetic dipole and electric quadrupole can be written in a form similar to that of the muon. Nevertheless, one expects the dimension 6 operator to be suppressed with respect to the dimension 4 operators by a factor of $M_W^2/(\Lambda = 1 \text{ TeV})^2 \simeq 10^{-2}$. Higher dimension operators correspond to momentum dependence [52] in the form factors which are not so important in the process we are considering so are not included. At tree level the standard model (SM) requires $g_1^Z = \kappa_V = 1$ and $\lambda_V = 0$. Typically, radiative corrections from heavy particles will change κ_V by about $\sim 10^{-2}$ and λ_V by about $\sim 10^{-3}$ [53]. In particular, the contributions from a 200 GeV top quark and a 150 GeV Higgs boson to κ_V and λ_V are of order 10^{-3} .

The nearness of the ρ parameter to 1 implies an $SU(2)$ invariance of the weak interaction. Imposing this from the outset implies a relationship between the parameters reducing the number of parameters from 5 to 3 [54]. $SU(2)$ invariance is the basis of the other two parametrizations we mention. The difference between the two is that in the first, the Higgs

boson is heavy so that Goldstone bosons are nonlinearly realized while in the second, the Higgs bosons are light, leading to linearly realized Goldstone bosons.

B. Non-Linearly Realized Higgs Sector

The second commonly used parametrization is the Chiral Lagrangian approach [48,55]. A custodial $SU(2)$ is assumed which is supported to high accuracy by the nearness of the ρ parameter to 1. This approach assumes that the theory has no light Higgs particles and the electroweak gauge bosons interact strongly with each other above approximately 1 TeV. This can be described by a non-linear realization of the $SU(2) \times U(1)$ symmetry in a chiral Lagrangian formalism leading to the effective Lagrangian:

$$L = -ig \frac{L_{9L}}{16\pi^2} \text{Tr}[W^{\mu\nu} D_\mu \Sigma D_\nu \Sigma^\dagger] - ig' \frac{L_{9R}}{16\pi^2} \text{Tr}[B^{\mu\nu} D_\mu \Sigma^\dagger D_\nu \Sigma] + gg' \frac{L_{10}}{16\pi^2} \text{Tr}[\Sigma B^{\mu\nu} \Sigma^\dagger W_{\mu\nu}] \quad (2)$$

where $W_{\mu\nu}$ and $B_{\mu\nu}$ are the $SU(2)$ and $U(1)$ field strength tensors given in terms of $W_\mu \equiv W_\mu^i \tau_i$ by

$$\begin{aligned} W_{\mu\nu} &= \frac{1}{2}(\partial_\mu W_\nu - \partial_\nu W_\mu + \frac{i}{2}g[W_\mu, W_\nu]) \\ B_{\mu\nu} &= \frac{1}{2}(\partial_\mu B_\nu - \partial_\nu B_\mu)\tau_3, \end{aligned} \quad (3)$$

$\Sigma = \exp(iw^i \tau^i / v)$, $v = 246$ GeV, w^i are the would-be Goldstone bosons that give the W and Z their masses via the Higgs mechanism, and the $SU(2)_L \times U(1)_Y$ covariant derivative is given by $D_\mu \Sigma = \partial_\mu \Sigma + \frac{1}{2}igW_\mu^i \tau^i \Sigma - \frac{1}{2}ig'B_\mu \Sigma \tau^3$. The Feynman rules are found by going to the unitary gauge where $\Sigma = 1$. Note that often in the literature the coefficient $1/16\pi^2$ is replaced with v^2/Λ^2 . L_{10} contributes to the gauge boson self energies where it is tightly constrained to $-1.1 \leq L_{10} \leq 1.5$ [14] so we will not consider it further. New physics contributions are expected to result in values of $L_{9L,9R}$ of order 1 [48].

C. Linearly Realized Higgs Sector

In the linear realization scenario [56] the Higgs doublet field Φ is included in the low energy particle content. This approach assumes that any deviations from the Standard Model due to new physics manifests themselves in $SU(3) \times SU(2) \times U(1)$ gauge invariant singlet operators. There are 7 relevant operators of which four are stringently constrained by the high precision low energy and Z boson data [15]. The remaining three can give rise to non-standard couplings

$$\mathcal{L} = ig' \frac{\varepsilon_B}{\Lambda^2} (D_\mu \Phi)^\dagger B^{\mu\nu} (D_\nu \Phi) + ig \frac{\varepsilon_W}{\Lambda^2} (D_\mu \Phi)^\dagger W^{\mu\nu} (D_\nu \Phi) \quad (4)$$

$$+ \frac{2i}{3} \frac{L_\lambda}{\Lambda^2} g^3 \text{Tr}[W_{\mu\nu} W^{\nu\rho} W_\rho^\mu] \quad (5)$$

It seems most likely that anomalous couplings in the light Higgs linear scenario would best be studied by measuring the properties and couplings of the Higgs boson directly. In any case the parameters from this approach can be rewritten in terms of the parameters of the first two Lagrangians discussed.

The parameters from the three Lagrangians can be mapped onto each other:

$$\begin{aligned} g_1^Z &= 1 + \frac{e^2}{32\pi^2 s_w^2 c_w^2} (L_{9L} + \frac{2s^2 L_{10}}{(c_w^2 - s_w^2)}) &= 1 + \frac{e^2}{s_w^2} \frac{v^2}{4\Lambda^2} (\frac{\varepsilon_W}{c_w^2}) \\ \kappa_z &= 1 + \frac{e^2}{32\pi^2 s_w^2 c_w^2} (L_{9L} c_w^2 - L_{9R} s_w^2) + \frac{4s_w^2 c_w^2}{(c_w^2 - s_w^2)} L_{10} &= 1 + \frac{e^2}{s_w^2} \frac{v^2}{4\Lambda^2} (\varepsilon_W - \frac{s_w^2}{c_w^2} \varepsilon_B) \\ \kappa_\gamma &= 1 + \frac{1}{32\pi^2} \frac{e^2}{s_w^2} (L_{9L} + L_{9R} - 2L_{10}) &= 1 + \frac{e^2}{s_w^2} \frac{v^2}{4\Lambda^2} (\varepsilon_W + \varepsilon_B) \\ \lambda_\gamma &= \lambda_z &= (\frac{e^2}{s_w^2}) L_\lambda \frac{M_W^2}{\Lambda^2} \end{aligned}$$

Dropping the L_{10} term, the linear and non-linear realizations are obtained from each other by identifying $L_{9L} = 2\varepsilon_W$ and $L_{9R} = 2\varepsilon_B$. In the non-linear realization, the counterpart of L_λ is higher dimension.

III. CALCULATIONS AND RESULTS

To study the process $e^+e^- \rightarrow \ell^\pm \nu q \bar{q}'$ we included all tree level diagrams to the four fermion final states. There are 10 diagrams contributing to the $e^+e^- \rightarrow \mu^\pm \nu_\mu q \bar{q}'$ final state

which are shown in Fig. 1. The gauge boson coupling we are studying is present in diagram (1a). This, along with diagram (1b) are the diagrams responsible for real W production. For the $e^\pm \nu_e q \bar{q}'$ final state the 10 diagrams shown in Fig. 2 must also be included with those of Fig. 1 for a total of 20 diagrams. Diagram (2a) includes a TGV. The diagrams with t-channel photon exchange make large contributions to single W production due to the pole in the photon propagator which can be used to isolate the $WW\gamma$ vertex from the WWZ vertex [39,46].

We include final width effects by using vector boson propagators of the form $(s - M_V^2 + i\Gamma_V M_V)^{-1}$ which yields a gauge invariant result. Strictly speaking we should have included a momentum dependent vector boson width but this leads to problems with gauge invariance [30,37,58,57]. Although a number of solutions to this problem have been discussed [30,37,58] the difference between our treatment and more rigorous ones have a totally negligible effect on the TGV sensitivities we obtain from our analysis. A more rigorous treatment must of course be included in Monte Carlo simulations that will be used to analyze real experimental data. We will find that the non-resonant diagrams make non-negligible contributions to cross sections and are dependent on the kinematic cuts used in the analysis. These contributions are at least as important as electroweak radiative corrections.

To evaluate the cross-sections and different distributions, we used the CALKUL helicity amplitude technique [59] to obtain expressions for the matrix elements and performed the phase space integration using Monte Carlo techniques [60]. The expressions for the helicity amplitudes are lengthy and unilluminating so we do not include them here. To obtain numerical results we used the values $\alpha = 1/128$, $\sin^2 \theta = 0.23$, $M_Z = 91.187$ GeV, $\Gamma_Z = 2.49$ GeV, $M_W = 80.22$ GeV, and $\Gamma_W = 2.08$ GeV. In our results we included two generations of quarks and took them to be massless. In order to take into account finite detector acceptance we require that the lepton and quarks are at least 10 degrees away from the beam and have at least 10 GeV energy unless otherwise noted.

In principle we should include QED radiative corrections from soft photon emission and the backgrounds due to a photon that is lost down the beam pipe [40,41,43]. These

backgrounds are well understood and detector dependent. We assume the approach taken at LEP, that these effects can best be taken into account by the experimental collaborations. In any case, although initial state radiation must be taken into account their inclusion does not substantially effect the bounds we obtain and therefore our conclusions.

In figure 3 and Table I we show the cross sections for the processes $e^+e^- \rightarrow \ell^\pm \nu_\ell q\bar{q}'$ for different applications of cuts on the invariant mass of the lepton-neutrino pair and the $q\bar{q}'$ pair; $|M_{(\ell\nu),(q\bar{q}')} - M_W| < 5 \text{ GeV}$ where $M_{(\ell\nu),(q\bar{q}')}$ is the invariant mass of the $\ell\nu$ and $q\bar{q}'$ pair respectively. Imposing the cut on one fermion pair gives the single W cross section and imposing the cut on both fermion pairs gives the W -pair production cross section. In both cases the single W and W pair thresholds are clearly seen. Although the single W production cross section is nonzero below the W -pair production threshold, it is still too small to obtain adequate statistics to perform studies of W boson properties. In general the electron mode has a larger cross-section than the muon mode. The difference is small at 175 GeV but becomes increasingly larger at higher energy as the t-channel photon exchange becomes increasingly important, reaching a factor of 5 at 1 TeV. For the muon mode the invariant mass cuts reduce the cross-section by 10% to 20% depending on \sqrt{s} irrespective of whether the cut is on $M_{\ell\nu}$ or $M_{q\bar{q}'}$. The relatively small effect of these cuts verifies the dominance of the resonant diagrams on the total cross section.

For the electron mode the results are similar when the $|M_{e\nu} - M_W| < 5 \text{ GeV}$ cut is imposed which constrains the $e\nu$ pair to be on the W mass-shell. However when $|M_{q\bar{q}'} - M_W| < 5 \text{ GeV}$ (ie. $W \rightarrow q\bar{q}'$) the cross section is significantly larger than the previous case due to the enhancement arising from the non-resonant t-channel photon exchange diagrams of fig. 2. With appropriate kinematic cuts this can be used to study single- W production [46].

Despite the relative smallness of the off-resonance contributions to the muon mode they still contribute up to 30% of the cross section at 1 TeV. Clearly, they must be properly included when making high precision tests of standard model processes. For the electron mode they are even more important and are interesting in the context of single W production.

A. Distributions

The above points can be amplified by examining kinematic distributions. In addition, since our goal is to extract measurements of the TGV's, we must explore which distributions are most sensitive to anomalous couplings. For descriptive purposes we will show various distributions for $\sqrt{s} = 500$ GeV.

We begin by showing in Fig. 4 the invariant mass distributions for the $e\nu$ ($M_{e\nu}$) and $\mu\nu$ ($M_{\mu\nu}$) pairs for left and right handed initial electron polarization. As the unpolarized cross sections are dominated by the left handed electrons they are quite similar to them, so we do not include them separately. In addition, the $q\bar{q}$ invariant mass distributions for left handed initial electrons are similar to the $M_{\mu\nu}$ distributions. Since there are differences for the right handed initial electron distributions, these distributions are also included. The differences in these cross sections reflects the differences and relative importance in the Feynman diagrams that contribute to a process. Although the cross sections and the sensitivities to the TGV's are dominated by the production of real W 's one can see that off-resonance production of the $\ell\nu q\bar{q}'$ final state can be quite sensitive to anomalous couplings. We will explore this in a later section. The effects are especially pronounced for the $e\nu q\bar{q}'$ final state where there is the possibility of single W production which is discussed elsewhere [39,46].

We examined numerous distributions with the purpose of finding the distributions and isolating the regions of phase space most sensitive to anomalous couplings;

$$\frac{d\sigma}{dp_{T_W}}, \quad \frac{d\sigma}{dp_{T_\mu}}, \quad \frac{d\sigma}{dp_{E_\mu}}, \quad \frac{d\sigma}{d\cos\theta_{eW}}, \quad \frac{d\sigma}{d\cos\theta_{e\mu}} \quad \text{etc.} \quad (6)$$

There is, of course, overlap among the regions of interest in these distributions. To gauge the sensitivity of these distributions to the TGV's we typically divided them into 4-bins and performed a χ^2 analysis. For $\sqrt{s} = 500$ GeV and integrated luminosity of 50 fb^{-1} we found, for example, that the κ 's could be measured to a couple of percent at 95% confidence level. It turns out that this is not competitive with a more sophisticated analysis of angular distributions we will describe below. Generally, this is because the phase space regions

with the highest statistics are least sensitive to anomalous couplings and tend to overwhelm deviations while the regions most sensitive to TGV's have poor statistics.

For the purpose of understanding W -boson properties the most interesting distributions are the various angular distributions. To understand this better it is useful to first consider the W pair production cross section without decays to fermions [61,62]. To leading order the amplitude for W pair-production is given by three diagrams; via an s-channel photon, an s-channel Z^0 and a t-channel neutrino exchange. The cross sections at different $\sqrt{s} = 200, 500$, and 1000 GeV, for $W_L W_L$, $W_L W_T$, and $W_T W_T$, different initial state polarizations, and as a function of the W scattering angle are shown in Fig. 5 [2]. For the initial state $e_R^- e_L^+$ only the first two diagrams contribute which at high energy is dominated by longitudinal W (W_L) production. Due to the delicate cancellations between the diagrams it is W_L production which is most sensitive to anomalous couplings. In contrast, the cross section for the $e_L^- e_R^+$ initial state produces both transverse and longitudinal W bosons with comparable rates. The e_L^- cross section is dominated by a peak in the forward direction with respect to the incoming e^- associated with the t-channel neutrino exchange which is made up entirely of transverse W production. This contribution is relatively insensitive to new physics. The cross sections in the backward direction includes sizable longitudinal W production accounting for about 25% of the total cross section in the backward hemisphere. However, in the backward direction where the s-channel diagrams contribute substantially, the cross section for e_R^- is always quite small. For e_R^- there is a large change in the magnitude of the cross-section but only a small change in its shape.

Any disruption of the delicate gauge theory cancellations leads to large changes to the standard model results. For W_L production amplitudes the enhancements can be a factor of (s/M_W^2) . This is shown in Fig. 6 where the angular distribution of the outgoing W is plotted for several values of anomalous couplings at $\sqrt{s} = 500$ GeV.

Because it is the longitudinal W production which is most sensitive to anomalous couplings, and because the cross section is dominated by transverse W production it is crucial to disentangle the W_L from the W_T *background*. The most convenient means of doing so

makes use of the angular distribution of the W decay products. Defining θ_ℓ and θ_q as the angle between the ℓ or q and the W momentum measured in the W rest frame, the angular distribution in θ peaks about $\cos\theta = 0$ for longitudinally polarized W bosons and at forward or backward angles for transversely polarized bosons. In addition the parity violation of the W couplings distinguishes the two polarization states adding to the effectiveness of the decay as a polarimeter. Thus the angular distributions can be used to extract information about the W boson polarizations. In Fig. 7 we show the angular distributions for the outgoing quark with respect to the W direction (θ_q) for the three bins in the W scattering angle, $\cos\Theta_W < -0.9$, $-0.05 < \cos\Theta_W < 0.05$ and $\cos\Theta_W > 0.9$, (where we take Θ_W to be the W^- angle with respect to the incoming e^-) for the process $e^+e^- \rightarrow \mu^+\nu_\mu q\bar{q}'$ at $\sqrt{s} = 500$ GeV with the initial electron unpolarized. Several values of κ_V and λ_V are included to demonstrate the sensitivity of the distributions to anomalous couplings. The figure shows the dominance of the transverse W polarization at forward angles and the increasing importance of the W longitudinal polarization at $\cos\Theta_W = 0$. Note also the relative lack of sensitivity to anomalous couplings for the forward, dominantly transverse W 's and how the sensitivity increases as the scattering angle increases and longitudinal W 's contribute a larger fraction of the cross section.

We have shown the $d^2\sigma/d\cos\Theta_W d\cos\theta_q$ distribution as it displays the most dramatic change in the shape of the distributions. However, interference between the transverse and longitudinal W 's also depends on the azimuthal angle so that the azimuthal angular distribution also shows changes in its shape, albeit smaller. One finds similar effects in the angular distributions for the decay $W \rightarrow \ell\nu$.

B. Maximum Likelihood fit of 5-dimensional angular distribution

The approach which makes the most complete use of information in an event is the maximum likelihood method. Based on the observations of the previous section we perform a maximum likelihood fit based on the 5 angles [29,31]; Θ , the W^- scattering angle with

respect to the initial e^+ direction, θ_{qq} , the polar decay angle of the q in the W^- rest frame using the W^- direction as the quantization axis, ϕ_{qq} , the azimuthal decay angle of the q in the W^- rest frame, and $\theta_{\ell\nu}$ and $\phi_{\ell\nu}$ are the analogous angles for the lepton in the W^+ rest frame. The azimuthal angles are defined as the angle between the normal to the reaction plane, $n_1 = p_e \times p_W$ and the plane defined by the W decay products, $n_2 = p_q \times p_{\bar{q}}$. The angles are shown in Fig. 8. For the $q\bar{q}$ case there is an ambiguity since we cannot tell which hadronic jet corresponds to the quark and which to the antiquark. We therefore include both possibilities in our analysis.

To implement the maximum likelihood analysis we divided each of Θ , θ_{qq} , ϕ_{qq} , $\theta_{\ell\nu}$, and $\phi_{\ell\nu}$ into four bins so that the entire phase space was divided into $4^5 = 1024$ bins. With this many bins some will not be very populated with events so that it is more appropriate to use Poisson statistics rather than Gaussian statistics. This leads naturally to the maximum likelihood method. The change in the log of the Likelihood function is given by

$$\delta \ln \mathcal{L} = \sum [-r_i + r_i \ln(r_i) + \mu_i - r_i \ln(\mu_i)] \quad (7)$$

where the sum extends over all the bins and r_i and μ_i are the predicted number of non-standard model and standard model events in bin i respectively, given by

$$r_i = L \int_{\Delta\Theta} \int_{\Delta\theta_{qq}} \int_{\Delta\phi_{qq}} \int_{\Delta\theta_{\ell\nu}} \int_{\Delta\phi_{\ell\nu}} \frac{d^5\sigma}{d \cos \Theta d \cos \theta_{qq} d \phi_{qq} d \cos \theta_{\ell\nu} d \phi_{\ell\nu}} d \cos \Theta d \cos \theta_{\ell\nu} d \phi_{\ell\nu} d \cos \theta_{qq} d \phi_{qq} \quad (8)$$

where L is the expected integrated luminosity. The 68% and 95% confidence level bounds are given by the values of anomalous couplings which give a change in $\ln \mathcal{L}$ of 0.5 and 2.0 respectively.

Ideally, one would perform the analysis on an event by event basis but to simplify our calculations we used a five dimensional angular distribution. To check the sensitivity to binning we varied the number of dimensions and bins used in our fits. For this binning approach we found that the results converged to the tightest bounds using the five dimensional distribution and 4 bins per dimension. In a few test runs for special cases of kinematic

cuts we calculated the likelihood function on an event by event basis and found that the sensitivities improved a small amount over the 5 dimensional distribution case described above.

The results we obtained are based solely on the statistical errors based on the integrated luminosity we assume for the various cases. To include the effects of systematic errors using the maximum likelihood approach requires an unweighted Monte Carlo simulation through a realistic detector. Since we did not have the facilities to do this we attempted a simplified estimate of systematic errors using χ^2 analysis to make our estimates. We assumed a systematic error of 5% of a measurement which we combined in quadrature with the statistical error. In general the systematic errors are negligible compared to the statistical errors. The only times they made a measurable difference was for the high luminosity cases of the 500 GeV and 1 TeV NLC, and even there the effect was quite small. It is straightforward to see why this is so; with so many bins the number of events per bin is quite small resulting in a large statistical error. Thus, it appears that the total errors will be dominated by the statistical errors but clearly, a full detector Monte Carlo must be performed to properly understand the situation.

C. Unpolarized Results

A thorough analysis of gauge boson couplings would allow all five parameters in the Lagrangian to vary simultaneously to take into account cancellations (and correlations) among the various contributions. This approach is impractical, however, due to the large amount of computer time that would be required to search the parameter space. Instead we show 2-dimensional contours for a selection of parameter pairs to give a sense of the correlations. For the case of the Chiral Lagrangian where the global SU(2) symmetry imposes relations between the parameters and where we restrict ourselves to dimension four operators the parameter space reduces to 2 dimensions.

1. $\sqrt{s} = 175 \text{ GeV}$

For the LEP200 collider we study the sensitivity to the gauge boson couplings using the expected machine parameters of $\sqrt{s} = 175 \text{ GeV}$ and an integrated luminosity of 500 pb^{-1} . These results do not have a cut on $M_{\ell\nu}$ or $M_{q\bar{q}}$ since for these energies the cuts have virtually no effect on the sensitivities except for the electron mode involving the $WW\gamma$ vertex where the effect is still quite small. The 95% confidence limits for the $g_Z^1 - \kappa_Z$, $\kappa_\gamma - \kappa_Z$, $\kappa_\gamma - \lambda_\gamma$, and $\kappa_Z - \lambda_Z$ planes are shown in Fig. 9 and for the $L_{9L} - L_{9R}$ plane is shown in Fig. 10. The sensitivities of the couplings, varying one parameter at a time, are summarized in Table II. In each of these figures, contours are shown for the muon mode alone and then for the combined results of the e and μ modes with both charge possibilities. We also show contours for a reduced integrated luminosity of 300 fb^{-1} . For the L_{9L} vs L_{9R} plot we show contours for both the electron and muon modes since there is a visible difference for the two modes. By combining the four lepton modes the couplings can be measured to $\delta g_Z^1 = \pm 0.22$, $\delta \kappa_Z = \pm 0.2$, $\delta \kappa_\gamma = \pm 0.27$, $\lambda_Z = \pm 0.18$, $\lambda_\gamma = \pm 0.3$, $\delta L_{9L} = \pm 55$, and $\delta L_{9R} = \sim \pm 300$. If the results of the four LEP experiments could be combined these results could be reduced further. Nevertheless, these limits are at the very least an order of magnitude less sensitive than would be required to see the effects of new physics through radiative corrections and are comparable to the sensitivities that could be achieved at a high luminosity Tevatron upgrade. It is therefore unlikely, that new physics will reveal itself at LEP200 through precision measurements of the TGV's.

2. $\sqrt{s} = 500 \text{ GeV}$

For the $\sqrt{s} = 500 \text{ GeV}$ NLC option we assume an integrated luminosity of 50 fb^{-1} . At 500 GeV the results are most sensitive when we impose that the W 's are on mass-shell; ie. $|M_{\ell\nu} - M_W| < 10 \text{ GeV}$ and $|M_{q\bar{q}} - M_W| < 10 \text{ GeV}$. This is slightly more pronounced for the electron mode. After these cuts are imposed the electron and muon modes are essentially

identical. The 95% confidence limits for the $g_Z^1 - \kappa_Z$, $\kappa_\gamma - \kappa_Z$, $\kappa_\gamma - \lambda_\gamma$, and $\kappa_Z - \lambda_Z$ planes are shown in Fig. 11 and for the $L_{9L} - L_{9R}$ planes in Fig. 12. In each of these plots we show results for combining the four final states and the μ^+ mode alone. We also show contours for 10 fb^{-1} of integrated luminosity to show the effects of reducing the collider luminosity. The sensitivities, varying one at a time, are included in Table II.

Using the maximum likelihood analysis we find that κ_γ , κ_Z , λ_γ and λ_Z can be measured to better than ± 0.005 and g_Z^1 to roughly ± 0.01 at 95 % C.L. including the invariant mass cut and assuming 50 fb^{-1} integrated luminosity. If the integrated luminosity were reduced to 10 fb^{-1} the bounds become weaker by roughly a factor of two while combining all four modes improves the single mode bounds by roughly a factor of two. These measurements of g_Z^1 , κ_γ , and κ_Z should be precise enough to probe loop radiative corrections to the couplings. On the other hand the measurements of λ_γ and λ_Z are still an order of magnitude too large to see expected deviations from tree level values due to radiative corrections.

The $L_{9L} - L_{9R}$ contours are shown in Fig. 12. L_{9L} can be measured to ± 3 and L_{9R} to $\sim \pm 8$ using a single mode and to ± 1.5 and ± 4 respectively combining all four $\ell\nu q\bar{q}$ final states.

3. $\sqrt{s} = 1 \text{ TeV}$

For the 1 TeV NLC collider we assume an integrated luminosity of 200 fb^{-1} . The 95% C.L. sensitivity contours for the $g_Z^1 - \kappa_Z$ and $\kappa_\gamma - \kappa_Z$ are shown in Fig. 13. These results were obtained by imposing that the W 's be on mass shell; $|M_{\ell\nu} - M_W| < 10 \text{ GeV}$ and $|M_{q\bar{q}} - M_W| < 10 \text{ GeV}$. We do not bother showing the $\lambda_V - \kappa_V$ contours since they are uncorrelated (one parameter is least sensitive when the other is taken to be equal to zero) so it is sufficient to give the sensitivity when all other parameters are set to zero. The $L_{9L} - L_{9R}$ contours are shown in Fig 14. With these collider parameters g_Z can be measured to about ± 0.005 while κ_Z and κ_γ can be measured to about 10^{-3} . These measurements will be sensitive enough to test the standard model at the level of radiative corrections.

D. Initial State Polarization

In the earlier discussion of angular distributions we pointed out that reactions with different initial electron polarizations have different dependences on anomalous couplings [33]. In this section we explore the consequences of this behavior. We restrict our results to the dimension 4 operators where deviations are most likely to show up.

For the 500 GeV e^+e^- collider we took 25 fb^{-1} of integrated luminosity per polarization. We only include results for the four combined lepton modes. The 95% C.L. contours for the $g_Z - \kappa_Z$, $\kappa_\gamma - \kappa_Z$, and $L_{9L} - L_{9R}$ planes are shown in Fig. 15. Shown are contours for $e_L^- e^+$, $e_R^- e^+$, and unpolarized initial states. For the $g_Z - \kappa_Z$ plane there is not much difference in the shape of the contour for the different polarizations although the bounds improve slightly. On the other hand the different polarizations give much different dependences for the $\kappa_\gamma - \kappa_Z$ and $L_{9L} - L_{9R}$ contours. In the $\kappa_\gamma - \kappa_Z$ plane the right-handed electron polarizations give constraints orthogonal to the left-handed polarizations and unpolarized results. The unpolarized contours are aligned along the e_L^- contours which is not too surprising considering that $\sigma(e_L^-)$ dominates the right-handed contribution in the unpolarized cross-section. For the $L_{9L} - L_{9R}$ plane the left and right handed polarizations also give different dependences which would further constrain L_{9L} .

For the 1 TeV e^+e^- collider we took 100 fb^{-1} of integrated luminosity per polarization. The sensitivities are shown in Fig. 16. They are similar to, but more constraining, than the 500 GeV case so we do not comment further.

More important than the improvement in sensitivity is the usefulness of polarization for disentangling the nature of anomalous TGV's if deviations are observed.

E. Off Resonance Production

In this section we explore the information potential available from $\ell\nu q\bar{q}$ final states off the W resonance. Referring to the invariant mass distributions shown in Fig. 4 one sees

that there is considerable sensitivity to anomalous gauge boson couplings when the fermion pairs do not originate from real W production. We do not perform a rigorous analysis here but demonstrate that there is considerable information in the non-resonant production. In particular we do not consider possible backgrounds to non-resonant events and do not make any effort to optimize our cuts to enhance deviations from SM results.

We consider $\sqrt{s} = 200$ GeV, 500 GeV, and 1 TeV for both the $e\nu q\bar{q}$ and $\mu\nu q\bar{q}$ final states and include initial state polarization when appropriate. We based our results on the total cross-section upon imposing the cuts $M_{ff'} < M_W - 15$ GeV and $M_{ff'} > M_W + 15$ GeV where $M_{ff'}$ is the invariant mass of the final state fermion pairs and ff' stands for either $\ell\nu$ or $q\bar{q}$. These give rise to a large number of possibilities so we only present the “best” case when the four possible final states are combined for each energy.

1. $\sqrt{s} = 200$ GeV

For $\sqrt{s} = 200$ GeV we only considered unpolarized initial state electrons and positrons. The results here should be taken with a grain of salt due to the low number of events expected in these kinematic regions. For example, the standard model predicts, for an integrated luminosity of 500 fb^{-1} and combining all 4 final states, only 40 events when either $M_{\ell\nu} < M_W - 15$ GeV or $M_{\ell\nu} > M_W + 15$ GeV. With this warning, the optimum results occur for $M_{\ell\nu} < M_W - 15$ GeV and are given in Table III. The results are slightly weaker for the case $M_{q\bar{q}} < M_W - 15$ GeV. Although for a specific case, sensitivities may differ between the μ and e final states, they are generally quite similar. The case $M_{ff'} > M_W + 15$ GeV is not nearly as sensitive to anomalous couplings except for L_{gR} and κ_γ . These results, along with the previous ones which concentrated on the real W production, indicate that the results are dominated by real W production. The off-resonance results are roughly a factor of two to three weaker than those given previously for real W production and are not likely to contribute much to bounds on TGV’s at LEP200.

2. $\sqrt{s} = 500 \text{ GeV}$

For $\sqrt{s} = 500 \text{ GeV}$ and combining the four final states, the sensitivity is greatest when $M_{\ell\nu} > M_W + 15 \text{ GeV}$ except for a few cases. The results for $M_{q\bar{q}}$ cuts are slightly less sensitive. Considering either the e^\pm or μ^\pm final states separately we find that for the e^\pm final states the $M_{\ell\nu} > M_W + 15 \text{ GeV}$ case is more sensitive than the $M_{q\bar{q}} > M_W + 15 \text{ GeV}$ case while for the μ^\pm final states they are comparable. With $M_{\ell\nu} > M_W + 15 \text{ GeV}$ the e^\pm final states are more sensitive to couplings involving photons than the μ^\pm final states. In both cases when we take $M_{\ell\nu} > M_W + 15 \text{ GeV}$ the cross-section is dominated by the $q\bar{q}$ pair originating from an on-shell W . This gives us the case of single- W production which receives large contributions from t-channel photon exchange and hence it is more sensitive to the $WW\gamma$ coupling.

The NLC offers the possibility of initial electron polarization. We have included some representative results. An important difference between the two polarizations, which can be seen in Fig. 4, is that the cross-section with left handed electrons is about an order of magnitude larger than for right handed electrons. At the same time the right-handed cross-section is significantly more sensitive to anomalous couplings than the left-handed cross-section. There is therefore a tradeoff between sensitivity and statistics so that in some cases the bounds obtainable for the two polarizations are comparable. The unpolarized results offer no improvement over the polarized results since the right-handed cross-section is overwhelmed by the left-handed contribution. One exception to these comments is when we consider L_{9L} where the left-handed electrons are more constraining for L_{9L} .

3. $\sqrt{s} = 1 \text{ TeV}$

The results at 1 TeV are qualitatively similar to those at 500 GeV so we do not repeat the discussion of the previous section but only point out the few points that differ. Again, the highest sensitivity is for the constraint $M_{\ell\nu} > M_W + 15 \text{ GeV}$. The achievable bounds

for this case are included in Table III. They are typically 4 to 5 times more constraining than those obtainable at 500 GeV; less than 1% for κ_γ and κ_Z which is at the level of loop contributions from new physics.

One interesting difference is that the muon mode for right-handed initial electrons provides the most stringent constraints for many of the TGV couplings. As before, the electron final state offers the best measurements of κ_γ .

4. Comments on Off-Resonance Results

From the above results it is clear that, although the constraints that could be obtained from off-resonance production are not as tight as those obtained from on-shell W production, there is nevertheless considerable information contained in these events. It appears to us that the method that makes optimal use of each event is to calculate the probability of each event, irrespective of where it appears in phase space, and compute a likelihood function for the combined probabilities. The only experimental cuts that should be included are those that represent detector acceptance and that are introduced to eliminate backgrounds.

IV. CONCLUSIONS

We performed a detailed analysis of the measurement of tri-linear gauge boson couplings in the process $e^+e^- \rightarrow \ell^\pm \nu q \bar{q}$. We included all tree level contributions to this final state and included finite gauge boson width effects. The off-shell W contributions contribute from 20% for the μ mode at LEP200 to 30% and 100% for the electron mode at a 500 GeV and 1 TeV NLC respectively (with the kinematic cuts we used). Clearly, the non-resonant contributions must be included to properly account for the experimental situation.

To gauge the sensitivity of this process to anomalous gauge boson couplings we used the W decay distributions as a polarimeter to distinguish the longitudinal W modes, which are more sensitive to anomalous couplings, from the transverse modes. We implemented this through the use of a quintic differential cross section, with each angular variable divided

into 4 bins, and then calculating the likelihood function of non-standard model couplings as compared to the standard model. Using this approach we found that at LEP200 operating at 175 GeV and assuming integrated luminosity of 500 pb^{-1} , g_1^Z , κ_Z , κ_γ , λ_Z , and λ_γ could be measured to roughly ± 0.2 and L_{9L} and L_{9R} to ± 50 and ± 400 respectively. It is extremely unlikely that measurements of this precision would reveal anomalous couplings. At a 500 GeV NLC with an integrated luminosity of 50 fb^{-1} , g_1^Z , κ_V and λ_V , could be measured to roughly ± 0.01 , ± 0.005 and ± 0.0025 respectively and L_{9L} and L_{9R} to ± 1 and ± 4 respectively. At the 1 TeV NLC with 200 fb^{-1} the corresponding numbers are $\delta g_Z \sim \pm 0.05$, $\delta \kappa_{Z,\gamma} \sim \pm 10^{-3}$, $\delta L_{9L} \sim \pm 0.5$ and $\delta L_{9R} \sim \pm 1$. The 500 GeV NLC measurements are sensitive enough that they should be sensitive to loop contributions to the TGV's while the 1 TeV will be able to measure such effects.

We studied the sensitivity of the off-mass shell cross sections to anomalous couplings by imposing kinematic cuts on the invariant mass distributions of the outgoing fermion pairs. A cursory analysis found that the off-resonance cross section is relatively sensitive to anomalous couplings and that useful information could be extracted from this region of phase space.

Although the inclusion of W decays to fermions and the non-resonant diagrams does not alter the precision to which the TGV's can be measured they do change the cross sections and kinematic distributions at the same level as radiative corrections and must be taken into account for an accurate comparison between experiment and theory.

The optimal strategy to maximize the information contained in each event is to construct a likelihood function based on the four vector of each of the outgoing fermions on an event by event basis, putting them through a realistic detector simulation. This would make the best use of the information whether it be on the W resonance or not. Kinematic cuts should only be introduced to reduce backgrounds. Since the precision of these measurements is beyond the level of loop induced radiative corrections it is crucial that radiative corrections are well understood and included in event generators used in the study of these processes. Progress is being made along these lines as exemplified by the Monte Carlo event generators;

EXCALIBUR [41], WHOPPER, [63] EEW [43], WWF [44], and WGENP [64].

ACKNOWLEDGMENTS

The authors benefited greatly from many helpful conversations, communications, and suggestions during the course of this work with Tim Barklow, Genevieve Bélanger, Pat Kalyniak, Dean Karlen, and Paul Madsen. This research was supported in part by the Natural Sciences and Engineering Research Council of Canada and Les Fonds FCAR du Québec.

REFERENCES

- [1] D. Schaile, *Proceedings of the XXVII Int. Conf. on High Energy Physics*, eds. P.J. Bussey, I.G. Knowles, Glasgow, UK, 20-27 July 1994 (Inst. of Physics Publishing, 1995) p. 27.
- [2] K. Hagiwara *et al*, Nucl. Phys. **B282**, 253 (1987).
- [3] D. Zeppenfeld, Phys. Lett. **183B**, 380 (1987); D. Treille *et al*, Proceedings of the ECFA Workshop on LEP 200, ed. A. Böhm and W. Hoogland, Aachen (1986), CERN 87-08, vol.2, p.414. D.A. Dicus, K. Kallianpur, Phys. Rev. **D32**, 35 (1985); M.J. Duncan, G.L. Kane, Phys. Rev. Lett. **55**, 773 (1985); E.N.Argyres and C.G.Papadopoulos, Phys. Lett. **B263**, 298(1991).
- [4] G.Kane, J. Vidal, C.P. Yuan, Phys. Rev. **D39**, 2617 (1990), and references therein.
- [5] Some recent reviews on physics at high energy e^+e^- colliders are: M. Peskin, Proceedings of the 1987 SLAC Summer Institute on Particle Physics, SLAC-PUB-4601 (1988); D. Treille, Proceedings of the Workshop on Physics and Experiments with Linear e^+e^- Colliders, Waikoloa Hawaii, April 1993 (World Scientific; in press); A. Djouadi and P.M. Zerwas, Proceedings of *Beyond the Standard Model III*, ed. S. Godfrey and P. Kalyniak, Ottawa Canada, June 1992, (World Scientific, Singapore, 1993) p. 204.
- [6] A. Miyamoto, Proceedings of Workshop on Physics and Experiments with Linear e^+e^- Colliders, Waikoloa, Hawaii, ed. F.A. Harris, S.L. Olsen, S. Pakvasa, and X. Tata, (World Scientific, Singapore, 1994) p 141.
- [7] B. Wiik, Proceedings of the Workshop on Physics and Experiments with Linear e^+e^- Colliders, Waikoloa Hawaii, ed. F.A. Harris, S.L. Olsen, S. Pakvasa, and X. Tata, (World Scientific, Singapore, 1994).
- [8] Proceedings of the First Workshop on Japan Linear Collider (JLC), KEK, Oct 24-25, 1989, KEK Report 90-2 (1990); Proceedings of the Second Workshop on Japan Linear

- Collider, ed. S. Kawabata, Nov. 6-8, 1990 KEK Proceedings 91-10 Nov. 1991.
- [9] C. Ahn *et al.*, *Opportunities and Requirments for Experimentation at a Very High Energy e^+e^- Collider*, SLAC Report SLAC-0329 (1988);
 - [10] Proceedings of the Workshop on Physics at Future Accelerators, CERN Yellow Report 87-07 (1987).
 - [11] For a recent comprehensive review of trilinear gauge boson couplings see: H. Aihara *et al.*, To appear in *Electroweak Symmetry Breaking and Beyond the Standard Model*, eds. T. Barklow, S. Dawson, H. Haber and J. Siegrist (World Scientific), [hep-ph/9503425](#).
 - [12] For further recent reviews on TGV's see: I. Hinchliffe, To appear in the proceedings of the International Symposium on Vector Boson Self Interactions, UCLA, Feb 1-3, 1995, [hep-ph/9504206](#); F. Boudjema, To appear in the proceedings of *Beyond the Standard Model IV*, Lake Tahoe, California, Dec. 12-16, 1994, [hep-ph/9504409](#);
 - [13] C.P. Burgess, S. Godfrey, H. König, D. London, and I. Maksymyk, Phys. Rev. **D49**, 6115 (1994).
 - [14] S. Dawson and G. Valencia, Nucl. Phys. **B439**, 3 (1995).
 - [15] K. Hagiwara, S. Ishihara, R. Szalapski, and D. Zeppnefeld, Phys. Lett. **B283**, 353 (1992); Phys. Rev. **D48**, 2182 (1993).
 - [16] F. Abe *et al.* (CDF Collaboration), Phys. Rev. Lett. **74**, 1936 (1995); J. Ellison *et al.* (D0 Collaboration), Proceedings of the *DPF'94 Conference*, Albuquerque, NM, August 1994; H. Aihara, to appear in the Proceedings of the *International Symposium on Vector Boson Self-Interactions*, UCLA, February 1995; T.A. Fuess (CDF Collaboration), Proceedings of the *DPF'94 Conference*, Albuquerque, NM, August 1994; F. Abe *et al.* (CDF Collaboration), Proceedings of the *27th International Conference on High Energy Physics*, Glasgow, Scotland, July 20-27, 1994; F. Abe *et al.*, (CDF Collaboration), FERMILAB-Pub-95/036-E, submitted to Phys. Rev. Lett.; S. Abachi *et al.*, (D0

- Collaboration), FERMILAB-Pub-95/101-E, [hep-ex/9505007](#).
- [17] U. Baur and D. Zeppenfeld, Nucl. Phys. **B308**, 127 (1988); see also H. Aihara *et al.* Ref. [11].
 - [18] E. Yehudai, Phys. Rev. **D 41**, 33 (1990); **D44**, 3434 (1991); S.Y. Choi and F. Schrempp, Phys. Lett. **272B**, 149 (1991); I.F. Ginzburg, G.L. Kotkin, S.L. Panfil and V.G. Serbo, Nucl. Phys. **B228**, 285 (1983)
 - [19] S. Godfrey and K.A. Peterson, Carleton University report OCIP/C-92-7, [hep-ph/9302319](#).
 - [20] G. Couture, S. Godfrey, P. Kalyniak Phys. Rev. **D39**, 3239 (1989); Phys. Rev. **D42**, 1841 (1990); Phys. Lett. **B218**, 361 (1989).
 - [21] M. Raidal, University of Helsinki report HU-SEFT R 1994-16, [hep-ph/9411243](#); K. Cheung, S. Dawson, T. Han, and G. Valencia, Phys. Rev. **D51**, 5 (1995) ([hep-ph/9403358](#)); A. Queijeiro, Phys. Lett. **B193**, 354 (1987); K.J. Abraham and C.S. Kim, Phys. Lett. **B301**, 430 (1993); S.J. Brodsky, T.G. Rizzo, and I. Schmidt, SLAC-PUB-95-6904, [hep-ph/9505441](#).
 - [22] D. Choudhury and F. Cuyppers, [hep-ph/9312308](#).
 - [23] G. Couture and G. Bélanger, Phys. Rev. **D49**, 5720 (1994).
 - [24] G. Couture, S. Godfrey, and R. Lewis, Phys. Rev. **D45**, 777 (1992); G. Couture and S. Godfrey, Phys. Rev. **D49**, 5709(1994).
 - [25] S. Ambrosanio and B. Mele, Nucl. Phys. **B374**, 3 (1992).
 - [26] K. Hagiwara *et al.*, Nucl. Phys. **B365**, 544 (1991).
 - [27] G. Couture and S. Godfrey, Phys. Rev. **D50**, 5607(1994); K.J. Abraham, J. Kalinowski, and P. Ściepko, Proceedings of the XVII Warsaw Symposium on Elementary Particle Physics, Kazimierz, May 23-27, 1994, [hep-ph/9407223](#).

- [28] G.V. Borisov, V.N. Larin, and F.F. Tikhonin, *Zeit. Phys.* **C41**, 287 (1988).
- [29] T. Barklow, *Proceedings of the 1st Workshop on Physics with Linear Colliders*, Saariselka, Finland, Sept. 9-14 (1992); T. Barklow, *Proceedings of the DPF'94 Conference: 1994 Meeting of the Division of Particles and Fields of the APS*, Albuquerque, NM, Aug2-6, 1994.
- [30] C.G. Papadopoulos, CERN Report CERN-TH/95-46, [hep-ph/9503276](#).
- [31] R.L. Sekulin, *Phys. Lett.* **B338**, 369 (1994).
- [32] M. Bilenky, J.L. Kneur, F.M. Renard and D. Schildknecht, *Nucl. Phys.* **B409**, 22 (1993); G. Gounaris, J.L. Kneur, J. Layssac, G. Moutaka, F.M. Renard, and D. Schildknecht, *e^+e^- Collisions at 500 GeV, the Physics. Potential*, ed. P. Zerwas, DESY (Hamburg, 1991); K.J.F. Gaemers and M.R. van Velzen, *Z. Phys.* **C43**, 103 (1989); M. Diehl and O. Nachtmann, *Z. Phys.* **C62**, 397 (1994).
- [33] A.A. Pankov and N. Paver, *Phys. Lett.* **B324**, 224 (1994); **B346**, 115 (1995); A.A. Likhoded, A.A. Pankov, N. Paver, M.V. Shevlyagin and O.P. Yushchenko, UTS-DFT-93-22 (1993).
- [34] For a detailed review see W. Beenakker and A. Denner, *International Journal of Modern Physics* **A9**, 4837(1994).
- [35] P. Kalyniak, P. Madsen, N. Sinha, and R. Sinha, *Phys. Rev.* **D48**, 5081 (1993).
- [36] M. Gintner and S. Godfrey, *Phys. Lett.* **B**, (in press), [hep-ph/9510324](#).
- [37] Y. Kurihara, D. Perret-Gallix, and Y. Shimizu, *Phys. Lett.* **B349**, 367 (1995) ([hep-ph/9412215](#)); M. Nowakowski and A. Pilaftsis, *Z. Phys.* **C**; A. Aeppli, F. Cuypers and G. J van Oldenborgh, *Phys. Lett.* **B314**, 413 (1993).
- [38] F.A. Berends, R. Pittau, and R. Kleiss, *Nucl. Phys.* **B424**, 308(1994); G. Montagna, O. Nicrosini, G. Passarino, and F. Piccinini, CERN Report CERN-TH.7497/94 (1994,

- unpublished); D. Bardin, A. Leike, and T. Riemann, CERN Report CERN-TH.7478/94 (1994, unpublished), [hep-ph/9410361](#); G. Montagna, O. Nicrosini, G. Passarino, and F. Piccinini, CERN Report CERN-TH.7497/94 (1994; unpublished); J. Fujimoto *et al.*, KEP Report KEK 94-46; T. Ishikawa *et al.*, Proceedings of the *VIIth Workshop on High Energy Physics and Quantum Field Theory*, Sochi, Russia, Oct. 7-14 1992.
- [39] H. Iwasaki, Int. Journal of Mod. Phys. **A7**, 3291(1992); H. Neufeld, Z. Phys. **C17**, 145 (1983); E.N. Argyres and C.G. Papadopoulos, Phys. Lett. **263B**, 298 (1991); O. Philipsen, Z. Phys. **C54**, 643 (1992); G. Couture and J.N. Ng, Z. Phys. **C32**, 579 (1986); J.C. Romao and P. Nogueira, Z. Phys. **C42**, 263 (1989); O. Cheyette, Phys. Lett. **137B**, 431 (1984); C.G. Papadopoulos, Phys. Lett. **B333**, 202 (1994); E. Gabrielli, Mod. Phys. Lett. **A1**, 465 (1986).
- [40] O. Nicrosini and L. Trendadue, Nucl. Phys. **B318**, 1 (1989); L. Trentadue *et al.*, in : Z Physics at LEP1, ed. G. Altarelli, CERN Yellow report CERN 89-08 (CERN, Geneva, 1989) p129; D. Bardin, M. Bilenky, A. Olchevski, and T. Riemann, Phys. Lett. **B308**, 403 (1993);
- [41] F.A. Berends, R. Pittau, and R. Kleiss, Nucl. Phys. **B426**, 344(1994); [hep-ph/9409326](#); R. Pittau, [hep-ph/9406233](#).
- [42] W. Beenakker, K. Kolodziej, and T. Sack, Phys. Lett. **B258**, 469 (1991); W. Beenakker and A. Denner, DESY 94-051; W. Beenakker, F.A. Berends, and T. Sack, Nucl. Phys. **B367**, 287 (1991).
- [43] J. Fleischer, F. Jegerlehner and M. Zralek, Z. Phys. **C42**, 409 (1989); J. Fleischer, F. Jegerlehner, K. Koodziej, and G.J. van Oldenborgh, preprint PSI-PR-94-16 (1994; unpublished), [hep-ph/9405380](#).
- [44] G. Jan van Oldenborgh, P.J. Franzini, and A. Borrelli, [hep-ph/9402298](#).
- [45] D. Bardin *et al.*, CERN Report CERN-TH.7295/94, [hep-ph/9406340](#); J. Fujimoto

- et al.*, hep-ph/9407308; G. Montagna *et al.*, CERN Report CERN-TH.7497/94, hep-ph/9411332; Yu.L. Dokshitzer, V.A. Khoze, L.H. Orr, and W.J. Stirling, Phys. Lett. **B313**, 171 (1993).
- [46] M. Gintner, S. Godfrey and G. Couture, in preparation.
- [47] For recent reviews of effective Lagrangians see: M.B. Einhorn Proceedings of the *Workshop on Physics and Experiments with Linear e^+e^- Colliders*, eds. F.A. Harris *et al.*, Waikoloa Hawaii, April 26-30, 1993 (World Scientific, 1994) p. 122; F. Boudjema, *ibid*, p.712.
- [48] J. Bagger, S. Dawson, and G. Valencia, Nucl. Phys. **B399**, 364 (1993).
- [49] K. Gaemers and G. Gounaris, Z. Phys. **C1**, 259 (1979).
- [50] K.-i Hikasa Phys. Rev. **D33**, 3203 (1986); K. Hagiwara *et al*, Nucl. Phys. **B282**, 253 (1987).
- [51] W.J. Marciano, A. Queijeiro, Phys. Rev. **D 33**, 3449 (1986); F. Boudjema, K. Hagiwara, C. Hamzaoui, and K. Numata, Phys. Rev. **D43**, 2223 (1991).
- [52] U. Baur and D. Zeppenfeld, Nucl. Phys. **B308**, 127 (1988).
- [53] W.A. Bardeen, R. Gastmans, and B. Lautrup, Nucl. Phys. **B46**, 319 (1972); E.N. Argyres *et al.*, Nucl. Phys. **B391**, 23 (1993); J. Papavassiliou and K. Philopides, Phys. Rev. **D48**, 4255 (1993); G. Couture and J.N. Ng, Z. Phys. **C35**, 65 (1987); G. Couture *et al.*, Phys. Rev. **D38**, 860 (1988).
- [54] M. Kuroda, F.M. Renard, and D. Schildnecht, Phys. Lett. **B183**, 366 (1987).
- [55] A. Longhitano, Nucl. Phys. **B188**, 118 (1981); T. Appelquist and C. Bernard, Phys. Rev. **D22**, 200 (1980); B. Holdom, Phys. Lett. **B258**, 156 (1991); A. Falk, M. Luke, and E. Simmons, Nucl. Phys. **B365**, 523 (1991); T. Appelquist and G.H. Wu, Phys. Rev. **D48**, 3235 (1993); see also J.F. Donoghue, E. Golowich, and B.R. Holstein, *Dynamics*

- of the Standard Model*, (Cambridge University Press, 1994).
- [56] W. Buchmüller and D. Wyler, Nucl. Phys. **B268**, 621 (1986); A. De Rújula, M.B. Gavela, P. Hernandez and E. Massó, Nucl. Phys. **B384**, 3 (1992)
 - [57] D. Zeppenfeld, J.A.M. Vermaseren and U. Baur, Nucl. Phys. **B375**, 3 (1992).
 - [58] U. Baur and D. Zeppenfeld, MAD/PH/878.
 - [59] R. Kleiss and W. J. Stirling, Nucl. Phys. **B262**, 235 (1985); Z.Xu D.-H.Zhang L. Chang Nucl. Phys. **B291**, 392 (1987).
 - [60] See for example V. Barger and R. Phillips, *Collider Physics*, (Addison-Wesley Publishing Company, 1987).
 - [61] M. Peskin, Proceedings of the 1987 SLAC Summer Institute on Particle Physics, SLAC-PUB-4601 (1988).
 - [62] D.L. Burke, Proceedings of the 1990 SLAC Summer Institute on Particle Physics, SLAC-PUB-5418 (1991).
 - [63] H. Anlauf *et al.* Proceedings of Workshop on Physics and Experiments with Linear e^+e^- Colliders, Waikoloa, Hawaii, ed. F.A. Harris, S.L. Olsen, S. Pakvasa, and X. Tata, (World Scientific, Singapore, 1994) p 708.
 - [64] G. Montagne, O. Nicrosini, F. Piccinini, Comp. Phys. Commun. **90**, 141 (1995).

FIGURES

FIG. 1. The Feynman diagrams contributing to the process $e^+e^- \rightarrow \mu^+\nu_\mu q\bar{q}'$.

FIG. 2. The Feynman diagrams that contribute to the process $e^+e^- \rightarrow e^+\nu_\mu q\bar{q}'$ in addition to those of fig 1.

FIG. 3. $\sigma(e^+e^- \rightarrow \mu^+\nu_\mu q\bar{q}')$ and $\sigma(e^+e^- \rightarrow e^+\nu_e q\bar{q}')$ as a function of \sqrt{s} . A 10° cut away from the beam is imposed on charged final state fermions and no cut on their energy. In both cases the solid curve is the total cross section without any cuts on the $\ell\nu$ and $q\bar{q}'$ invariant masses. The dashed curves are for the cut $|M_{q\bar{q}'} - M_W| < 5$ GeV, the dotted curves for $|M_{\ell\nu} - M_W| < 5$ GeV and the dot-dashed curves for both $|M_{q\bar{q}'} - M_W| < 5$ GeV and $|M_{\ell\nu} - M_W| < 5$ GeV.

FIG. 4. Invariant mass distributions ($M_{\mu\nu}$, $M_{e\nu}$, and $M_{q\bar{q}'}$) of final state fermions in the processes $e^+e^- \rightarrow \mu^+\nu_\mu q\bar{q}'$ and $e^+e^- \rightarrow e^+\nu_e q\bar{q}'$ for $\sqrt{s} = 500$ GeV. Note the polarization of the initial electron. In all cases the solid line is the standard model cross section, the long-dashed line is for $\kappa_Z = 1.1$, the dotted line is for $\lambda_Z = 0.1$ and the dot-dashed line for $\kappa_\gamma = 0.5$.

FIG. 5. The angular distribution of the outgoing W^- with respect to the incoming electron for $\sqrt{s} = 200$ GeV, $\sqrt{s} = 500$ GeV, and $\sqrt{s} = 1$ TeV. The cross-section is given in units of $R = 4\pi\alpha^2/3s$. In all cases the top solid line is for $e_L^-e^+ \rightarrow W_TW_T$, the long-dashed line is for $e_L^-e^+ \rightarrow W_LW_T$, the medium-dashed line is for $e_L^-e^+ \rightarrow W_LW_L$, the short-dashed line is for the total of these three, the dotted line is for $e_R^-e^+ \rightarrow W_TW_T$, the dot-dashed line is for $e_R^-e^+ \rightarrow W_TW_L$, the double dot-dashed line is for $e_R^-e^+ \rightarrow W_LW_L$, and the bottom solid line is for the total of these last three. Note that there is no bottom-solid line for $\sqrt{s} = 500$ GeV.

FIG. 6. Angular distributions of W for $\sqrt{s} = 500$ GeV and (a) e_L^- and (b) e_R^- . In both cases the solid line is the SM result, the dashed line is for $\kappa_Z = 1.1$, the dotted line for $\lambda_\gamma = -0.1$ and the dot-dashed line for $\kappa_\gamma = 0.5$. The distributions were obtained from the full Monte Carlo by imposing the cut $|M_{q\bar{q}} - M_W| < 10$ GeV.

FIG. 7. Angular distributions of the outgoing quark with respect to the W^- direction in the W rest frame. In all cases the solid line is the SM result, the dashed line is for $\kappa_Z = 1.1$, the dotted line for $\lambda_Z = 0.1$ and the dot-dashed line for $\lambda_\gamma = -0.1$. The distributions were obtained from the full Monte Carlo by imposing the cut $|M_{q\bar{q}} - M_W| < 10$ GeV.

FIG. 8. Angle definitions used in our 5-dimensional angular distribution analysis. Θ is the W scattering angle, θ_{qq} and $\theta_{\ell\nu}$ are the decay angles in the W rest frames and ϕ_{qq} and $\phi_{\ell\nu}$ are the azimuthal angles, again in the W rest frames.

FIG. 9. 95% C.L. contours for sensitivity to anomalous couplings for $\sqrt{s} = 175$ GeV. In all cases the inner solid contour is obtained from combining all 4 lepton charge states for $L=500$ pb^{-1} , the heavy outer solid line is for the μ^+ mode alone for $L=500$ pb^{-1} , and the dotted contour is for the reduced luminosity case of $L=300$ pb^{-1} with all 4 modes combined.

FIG. 10. 95% C.L. contours for sensitivity to L_{9L} and L_{9R} for $\sqrt{s} = 175$ GeV. (a) The heavy solid line is for the μ^+ mode, the dotted line is for the e^+ mode and the inner solid line is for combining all four lepton charge states; all for $L=500$ pb^{-1} . (b) Both curves are from combining all four lepton charge states. The solid line is for $L=500$ pb^{-1} and the dotted line is for $L=300$ pb^{-1} .

FIG. 11. 95% C.L. contours for sensitivity to anomalous couplings for $\sqrt{s} = 500$ GeV. In all cases the inner solid contour is obtained from combining all 4 lepton charge states for $L=50$ fb^{-1} , the heavy solid line is for the μ^+ mode alone for $L=50$ fb^{-1} , and the dotted contour is for the reduced luminosity case of $L=10$ fb^{-1} with all 4 modes combined. These results were obtained by imposing that the W 's are on mass shell; $|M_{\ell\nu} - M_W| < 10$ GeV and $|M_{q\bar{q}} - M_W| < 10$ GeV.

FIG. 12. 95% C.L. contours for sensitivity to L_{9L} and L_{9R} for $\sqrt{s} = 500$ GeV. The inner solid line is obtained by combining all four lepton charge states and is for $L=50$ fb^{-1} , the heavy solid line is for all 4 modes and $L=10$ fb^{-1} and the dotted line is for the μ^+ mode alone for $L=50$ fb^{-1} . These results were obtained by imposing that the W 's are on mass shell; $|M_{\ell\nu} - M_W| < 10$ GeV and $|M_{q\bar{q}} - M_W| < 10$ GeV.

FIG. 13. 95% C.L. contours for sensitivity to anomalous couplings for $\sqrt{s} = 1$ TeV. In both cases the inner solid contour is obtained from combining all 4 lepton charge states for $L=200 \text{ fb}^{-1}$ and the dotted contour is for the reduced luminosity case of $L=50 \text{ fb}^{-1}$ with all 4 modes combined. The μ^+ contour for $L=200 \text{ fb}^{-1}$ lies on top of the dotted curves. These results were obtained by imposing that the W 's are on mass shell; $|M_{\ell\nu} - M_W| < 10 \text{ GeV}$ and $|M_{q\bar{q}} - M_W| < 10 \text{ GeV}$.

FIG. 14. 95% C.L. contours for sensitivity to L_{9L} and L_{9R} for $\sqrt{s} = 1$ TeV. The inner solid line is obtained by combining all four lepton charge states and is for $L=200 \text{ fb}^{-1}$ and the dotted line is for all 4 modes and $L=50 \text{ fb}^{-1}$. The μ^+ mode alone for $L=200 \text{ fb}^{-1}$ sits on top of the dotted contour. These results were obtained by imposing that the W 's are on mass shell; $|M_{\ell\nu} - M_W| < 10 \text{ GeV}$ and $|M_{q\bar{q}} - M_W| < 10 \text{ GeV}$.

FIG. 15. 95% C.L. contours for sensitivity to anomalous couplings for polarized initial state electrons for $\sqrt{s} = 500 \text{ GeV}$ and $L=25 \text{ fb}^{-1}$ per polarization and combining all four lepton charge states. In all cases the solid curves are for e_L^- , the dashed curves for e_R^- , and the heavy solid curve for unpolarized electrons (for a total of $L=50 \text{ fb}^{-1}$).

FIG. 16. 95% C.L. contours for sensitivity to anomalous couplings for polarized initial state electrons for $\sqrt{s} = 1 \text{ TeV}$ and $L=100 \text{ fb}^{-1}$ per polarization and combining all four lepton charge states. In all cases the solid curves are for e_L^- , the dashed curves for e_R^- , and the heavy solid curve for unpolarized electrons (for a total of $L=200 \text{ fb}^{-1}$).

TABLES

TABLE I. Cross-sections for $e^+e^- \rightarrow \mu^+\nu_\mu q\bar{q}'$ and $e^+e^- \rightarrow e^+\nu_e q\bar{q}'$ including cuts on the invariant masses of the outgoing fermion pairs, $M_{\ell\nu}$ and $M_{q\bar{q}'}$. The cross-sections are given in pb.

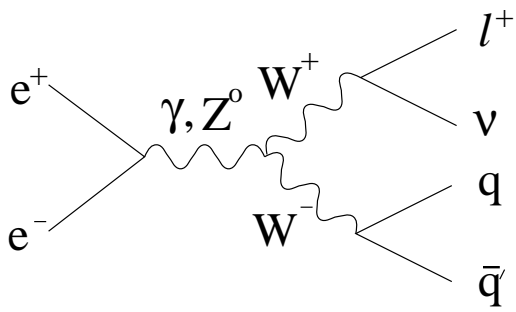
\sqrt{s} (GeV)	ℓ	no cut	$ M_{q\bar{q}} - M_W < 5 \text{ GeV}$	$ M_{\ell\nu} - M_W < 5 \text{ GeV}$	both cuts
175	μ	1.10	1.00	1.00	0.91
	e	1.15	1.04	1.01	0.91
500	μ	0.39	0.34	0.34	0.29
	e	0.62	0.53	0.34	0.29
1000	μ	0.077	0.063	0.064	0.052
	e	0.44	0.39	0.064	0.052

TABLE II. Sensitivities to anomalous couplings for the various parameters varying one parameter at a time. The values are obtained by combining the four lepton modes (e^- , e^+ , μ^- , and μ^+) and two generations of light quarks (ud , cs). The results are 95% confidence level limits.

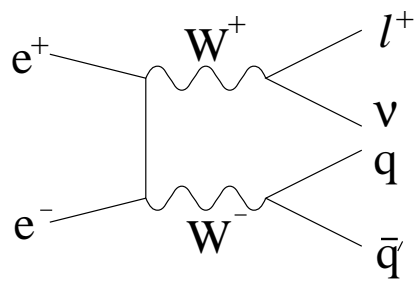
mode	L_{9L}	L_{9R}	δg_1^Z	$\delta \kappa_Z$	$\delta \kappa_\gamma$	λ_Z	λ_γ
$\sqrt{s} = 175 \text{ GeV}$, $L=500 \text{ pb}^{-1}$, no cuts on $M_{\ell\nu(q\bar{q})}$							
μ	± 110	$+920$ -420	$+0.45$ -0.44	$+0.39$ -0.38	$+0.58$ -0.48	$+0.36$ -0.35	$+0.61$ -0.50
e	$+120$ -110	$+620$ -440	$+0.44$ -0.43	$+0.40$ -0.38	$+0.58$ -0.52	$+0.37$ -0.35	$+0.62$ -0.49
combined	± 55	$+330$ -230	± 0.22	$+0.19$ -0.20	$+0.27$ -0.26	± 0.18	$+0.29$ -0.26
$\sqrt{s} = 500 \text{ GeV}$, $L=50 \text{ fb}^{-1}$, $ M_{\ell\nu(q\bar{q})} - M_W < 10 \text{ GeV}$							
μ	$+2.2$ -2.1	$+4.6$ -4.2	± 0.020	± 0.007	± 0.005	± 0.005	± 0.006
e	$+2.2$ -2.1	$+4.6$ -4.2	$+0.019$ -0.020	± 0.007	± 0.005	± 0.005	± 0.006
combined	$+1.1$ -1.0	$+2.2$ -2.1	± 0.0095	± 0.0035	± 0.0025	± 0.0025	± 0.0025
$\sqrt{s} = 1 \text{ TeV}$, $L=200 \text{ fb}^{-1}$, $ M_{\ell\nu(q\bar{q})} - M_W < 10 \text{ GeV}$							
μ	$+0.61$ -0.62	$+1.3$ -1.1	± 0.01	± 0.002	± 0.001	± 0.002	± 0.002
e	$+0.61$ -0.62	$+1.3$ -1.1	± 0.01	± 0.002	± 0.001	± 0.002	± 0.002
combined	± 0.28	$+0.62$ -0.56	± 0.0054	± 0.001	± 0.0006	± 0.0008	± 0.0008

TABLE III. Sensitivities to anomalous couplings based on off-resonance cross sections varying one parameter at a time. The values are obtained by combining the four lepton modes (e^- , e^+ , μ^- , and μ^+) and two generations of light quarks (ud , cs). The results are 95% confidence level limits. A dash signifies that the bound is significantly weaker than the others.

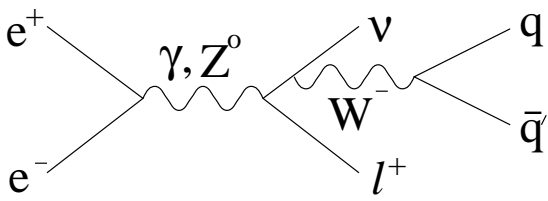
Initial State	cut	L_{9L}	L_{9R}	δg_{1Z}	$\delta \kappa_Z$	$\delta \kappa_\gamma$	λ_Z	λ_γ
$\sqrt{s} = 200 \text{ GeV}$, L=500 pb $^{-1}$								
e^-	$M_{\ell\nu} < M_W - 15 \text{ GeV}$	$^{+400}_{-320}$	$^{+520}_{-780}$	$^{+1.5}_{-1.1}$	$^{+1.1}_{-0.9}$	$^{+0.8}_{-1.0}$	$^{+1.0}_{-1.0}$	$^{+1.1}_{-0.7}$
$\sqrt{s} = 500 \text{ GeV}$, L=50 fb $^{-1}$								
e_L^-	$M_{\ell\nu} > M_W + 15 \text{ GeV}$	$^{+6.9}_{-7.2}$	$^{+8.9}_{-9.2}$	$^{+0.13}_{-0.18}$	$^{+0.056}_{-0.074}$	$^{+0.012}_{-0.012}$	$^{+0.026}_{-0.034}$	$^{+0.026}_{-0.041}$
e_R^-	$M_{\ell\nu} > M_W + 15 \text{ GeV}$	----	----	$^{+0.08}_{-0.24}$	$^{+0.03}_{-0.10}$	----	$^{+0.023}_{-0.033}$	$^{+0.034}_{-0.023}$
e^-	$M_{\ell\nu} > M_W + 15 \text{ GeV}$	$^{+10}_{-10}$	$^{+13}_{-13}$	$^{+0.15}_{-0.21}$	$^{+0.07}_{-0.10}$	$^{+0.016}_{-0.017}$	$^{+0.031}_{-0.038}$	$^{+0.033}_{-0.043}$
$\sqrt{s} = 1 \text{ TeV}$, L=200 fb $^{-1}$								
e_L^-	$M_{\ell\nu} > M_W + 15 \text{ GeV}$	$^{+2.4}_{-2.5}$	$^{+3.8}_{-3.9}$	$^{+0.038}_{-0.085}$	$^{+0.013}_{-0.014}$	$^{+0.005}_{-0.005}$	$^{+0.002}_{-0.002}$	$^{+0.003}_{-0.003}$
e_R^-	$M_{\ell\nu} > M_W + 15 \text{ GeV}$	----	$^{+0.062}_{-5.9}$	$^{+0.010}_{-0.102}$	$^{+0.010}_{-0.010}$	----	$^{+0.007}_{-0.007}$	$^{+0.007}_{-0.007}$
e^-	$M_{\ell\nu} > M_W + 15 \text{ GeV}$	$^{+3.4}_{-3.5}$	$^{+5.4}_{-5.6}$	$^{+0.047}_{-0.096}$	$^{+0.018}_{-0.021}$	$^{+0.007}_{-0.007}$	$^{+0.003}_{-0.003}$	$^{+0.003}_{-0.003}$



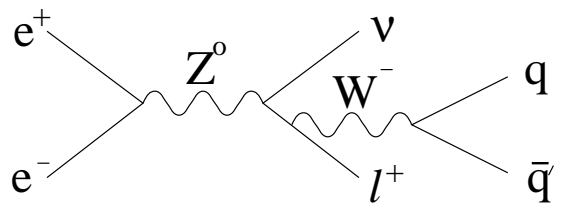
(a)



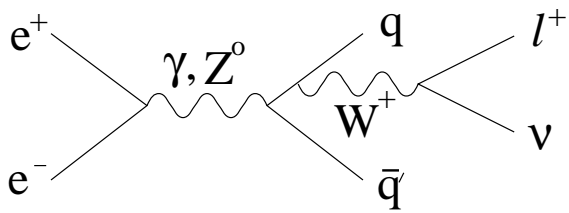
(b)



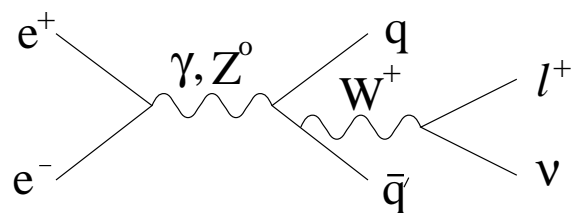
(c)



(d)



(e)



(f)

